Title

Onecut1 partially contributes to liver progenitor cell transition and acquisition of metastatic potential in hepatocellular carcinoma.

Yu Liu*[1, 2], Hiroaki Higashitsuji[1], Katsuhiko Itoh[1, 3], Kanji Yamaguchi[2], Atsushi Umemura[4], Yoshito Itoh[2], Jun Fujita[1, 5]

[1] Department of Clinical Molecular Biology, Graduate School of Medicine, Kyoto University, Kyoto 606-8507, Japan.

[2] Department of Gastroenterology and Hepatology, Kyoto Prefectural University of Medicine, Kyoto 602-8566, Japan.

[3] Educational Development Center, Kyoto University of Advanced Science, Kyoto 615-8577, Japan.

[4] Department of Pharmacology, Kyoto Prefectural University of Medicine, Kyoto 602-8566, Japan.

[5] Department of Molecular Genetics, Graduate School of Medicine, Kyoto University, Kyoto 606-8507, Japan.

Abstract

Metastasis-initiating cells are considered originating from stem cell-like cancer cells. In hepatocellular carcinoma, liver progenitor-like cells are reported to be derived from hepatocytes, indicating possible acquisition of metastatic potential during hepatocyte-to-cholangiocyte transdifferentiation. With a single cell RNA-seq study of hepatocyte-to-cholangiocyte transdifferentiation, we reveal that heptaocytes transit into liver progenitor cells and then differentiate into hepatocyte-like cells or cholangiocytes. In a hepatically differentiated hepatocellular carcinoma cell line, gradual expression of ONECUT1 represents liver progenitor cell transition, with low dose-dependent acquisition of metastatic potential, suggesting that tumor cells acquire metastatic potential in early stage of LPC transition.

Introduction

Metastasis is derived from a small proportion of disseminated tumor cells (Luzzi et al. 1998; Cameron et al. 2000), which are called metastasis-initiating cells. Metastasis-initiating cells are considered originating from a subset of stem cell-like cancer cells (Kouros-Mehr et al. 2008; Winslow et al. 2011; Chakrabarti et al. 2012; Cheung et al. 2013; Li et al. 2015), either cancer stem cells acquired metastatic traits, or cancer cells showed a regenerative stem-like phenotype.

In hepatocellular carcinoma (HCC), expression of cholangiocyte / liver progenitor cell (LPC) markers (i.e., *Krt19*, *Epcam*, *Sox9* and *Spp1*) indicates poor prognosis (Govaere et al. 2014; Chaudhary et al. 2018; Sun et al. 2013; Guo et al. 2012; Pan et al. 2003). However, the origin of LPCs in HCC, as well as origin of HCC itself, have been debated with conflicting evidence. In 2015, Mu *et al*. (Mu et al. 2015) reported that in both genotoxic and genetic models, HCC, including KRT19^{+} cells within tumors, arose exclusively from hepatocytes, indicating a crucial role of hepatocyte-to-cholangiocyte transdifferentiation in stemness acquisition.

One cut homeobox 1 (*Onecut1*, also known as *Hnf6*), is a key regulator during development but not postnatal regeneration of liver and biliary system (Clotman et al. 2002; Walter et al. 2014; Schaub et al. 2018). In fetal liver, ONECUT1 is weakly expressed in liver parenchyma and accumulates in ductal plate (Clotman et al. 2002). In adult liver, ONECUT1 is expressed in hepatocytes and is completely lost in mature cholangiocytes (Limaye et al. 2008). *Onecut1* knockout mice show absence of the gallbladder and interruption of bile duct with expansion of prematurely differentiated cholangiocytes, suggesting that *Onecut1* inhibits premature cholangiocytic differentiation (Clotman et al. 2002).

The function of *Onecut1* in HCC is poorly understood. Lazarevich *et al*. (Lazarevich et al. 2004) generated a highly invasive fast-growing dedifferentiated HCC from a well differentiated slow-growing HCC. In the dedifferentiated HCC, mRNAs of *Hnf1a*, *Hnf1b*, *Foxa3*, *Hnf4a* and *Onecut1* were downregulated. Recently, transient overexpression of *Onecut1* in HCC cell line was found to induce hepatic differentiation and inhibit

migration (Sun et al. 2016), but long-term effects of *Onecut1* overexpression remain unclear.

It is important to understand the molecular mechanisms underlying hepatocyte-to-cholangiocyte transdifferentiation for identification and treatment of metastasis-initiating cells in HCC. In this study, we report the roles played by *Onecut1* in regulating HCC cell fate and metastasis.

Results

ONECUT1 facilitates incomplete hepatocyte-to-cholangiocyte transdifferentiation.

Two cell lines hepaEP1 and hepaEP2 (hepaEPs) with a more epithelial-like morphology than the parental cells were subcloned from mouse HCC cell line hepa1-6 by limiting dilution (Figure 1A). In hepaEPs, mRNA of *Alb* was significantly elevated, indicating hepatic differentiation (Figure 1B). Elevated ALB secretion was verified by immunoblotting of serum-free culture supernatants and immunoprecipitants from serum-containing culture supernatants (Figure 1C, S1A). As hepatic differentiation in HCC cells is reported associating with suppressed proliferation, we examined proliferation of hepaEPs *in vitro* and *in vivo*. HepaEPs did not show a decreased proliferation either *in vitro* or in xenograft models (Figure S1B, S1C).

To investigate whether liver-enriched transcription factors play a role in hepatic differentiation of hepa1-6 cells, we analyzed mRNA expression of *Hnf1a*, *Hnf1b*, *Foxa1*, *Foxa2*, *Foxa3*, *Hnf4a*, *Onecut1*, *Cebpa* and *Cebpb*. *Foxa3*, *Hnf4a*, *Cebpa* and *Cebpb* were not detected, while only *Onecut1* mRNA showed a significant decrease in hepaEPs (Figure 1D). Decrease of ONECUT1 protein in hepaEPs were verified by immunoblotting of cell lysates (Figure 1E).

To understand role of *Onecut1*, we generated stable clones by introducing plasmids expressing ONECUT1 or 3FLAG-ONECUT1 into hepatically differentiated hepaEP1 cells (Figure 1F). Obtained cell lines and hepaEPs (hereafter collectively referred to as ONECUT1-EPs) were divided into 3 groups: ONECUT1^{low}-EPs (hepaEP1 and hepaEP2), ONECUT1^{int}-EPs (ONECUT1-EP1 and ONECUT1-EP2) and ONECUT1^{high}-

EPs (ONECUT1-EP7 and ONECUT1-EP9) with less than half, about equal, and more than 2-fold higher levels of ONECUT1 protein expression, respectively, compared with hepa1-6 cells (Figure 1G). In both ONECUT1^{int}-EPs and ONECUT1^{high}-EPs, mRNAs of *Alb*, *Afp* and *Ttr*, as well as ALB secretion showed significant reduction compared with hepaEP1 cells, suggesting that ONECUT1 expression suppresses hepatic differentiation (Figure 1H, S1D). As *Onecut1* plays a role in biliary development, we further investigated mRNA expression of cholangiocytic markers. *Krt19* showed exclusive upregulation in ONECUT1^{high}-EPs (Figure 1I).

Unexpectedly, downregulation of hepatic markers and upregulation of cholangiocytic markers were also observed in hepa1-6 cells transfected with *Onecut1* shRNA (ONECUT1-kd cells) (Figure S2A, S2B). Moreover, KRT19 protein was detected in ONECUT1-kd cells but not in ONECUT1^{high}-EPs with *Krt19* upregulation, indicating impaired cholangiocyte maturation in *Onecut1* overexpressed cells (Figure S2C, S2D, S2E).

In summary, gradual overexpression of ONECUT1 in ONECUT1^{low}-EPs causes suppression of hepatic markers and a higher dose-dependent elevation of *Krt19* mRNA, resulting in ONECUT1^{low}*Alb*^{high}*Krt19*^{low} hepatocyte-like cells, ONECUT1^{int}*Alb*^{low}*Krt19*^{low} dedifferentiated cells, and ONECUT1^{high}*Alb*^{low}*Krt19*^{high} cholangiocyte-like cells, which represents an incomplete multi-state hepatocyte-to-cholangiocyte transdifferentiation.

Single cell RNA-seq study reveals LPC transition during hepatocyte-to-cholangiocyte transdifferentiation.

Recently, a single cell RNA-seq study (Merrell et al. 2021) reported a more advanced hepatocyte-to-cholangiocyte transdifferentiation in DDC-treated *Smad4* mutant mice. However, cells under transdifferentiation were treated as a single cluster in the original report. To monitor the transcriptome kinetics during hepatocyte-to-cholangiocyte transdifferentiation, we tried to reanalyze the dataset at a higher resolution.

Single cell RNA-seq data were obtained from GSE157698, in which *Rosa*$^{YFP/YFP}$ *Smad4*$^{fl/+}$ control mice or *Rosa*$^{YFP/YFP}$ *Smad4*$^{fl/fl}$ mutant mice were injected with hepatocyte-specific AAV8-TBG-Cre, and then were treated with DDC. Bulk liver

parenchyma from control mice (GSM4885630 and GSM4885634), *eYFP*$^{+}$ bulk liver parenchyma from *Smad4* mutant mice (GSM4885631 and GSM4885635, *eYFP* > 0.2), and YFP^{+} sorted cells from both control mice (GSM4885632 and GSM4885636) and *Smad4* mutant mice (GSM4885633 and GSM4885637) were integrated and clustered. A total of 19 clusters were identified at a resolution of 0.7 (Figure S3A). As KRT19 protein was not expressed in ONECUT1^{high}*Alb*^{low}*Krt19*^{high} cells, mature cholangiocytes were defined as a *Krt19*$^{+}$ cluster present in control bulk liver parenchyma but not in control YFP+ cells due to incomplete hepatocyte-to-cholangiocyte transdifferentiation (Figure S3B). After cholangiocytes definition, *eYFP*$^{-}$ cells, contaminating hepatic stellate cells (cluster 10), endothelial cells and Kupffer cells (cluster 18) were omitted in further analysis (Figure S3C). As a result, *eYFP*$^{+}$ hepatocyte-derived cells formed a continuum rather than discrete clusters, including the estimated mature cholangiocytes (cluster 4) (Figure 2A).

Trajectory analysis and differentially expressed genes suggested that hepatocytes transit along clusters 3, 5, 0, and then branch into *Alb*^{high} hepatocyte-like cells (cluster 13), *Krt19*$^{+}$ estimated cholangiocytes (cluster 4), *Cdkn1a*$^{+}$ arrested cells (cluster 12), and proliferating cells (clusters 11, 15, 16), indicating bipotent-liver-progenitor-cell like ability and self-renewal capacity of cluster 0 (Figure 2B, 2C). According to the results, the hepatocyte-to-cholangiocyte transdifferentiation reveals a continuum of 3 major states: hepatocytes, LPC transition (including preLPC.1s, preLPC.2s, total LPCs which is further composed of LPCs, arrested LPCs and proliferating LPCs), and terminal differentiation (into hepatocyte-like cells or cholangiocytes) (Figure 2D). To assess the transdifferentiation levels, hepatic score (hep_score) and cholangiocytic score (chol_score) were respectively generated with hepatic or cholangiocytic markers (Franzén, Gan, and Björkegren 2019) (Figure S4). Along with the transdifferentiation continuum, chol_score gradually increased, while hep_score transiently increased before LPC transition, and then immediately decreased during LPC transition. Transdifferentiated hepatocyte-like cells showed a higher hep_score compared to LPCs (Figure 2E).

To confirm that *Smad4* mutation affects advanced hepatocyte-to-cholangiocyte transdifferentiation, we compared percentage of the continuum components between control mice and *Smad4* mutant mice. Consistent with the original report, accumulation of total LPCs, transdifferentiated hepatocyte-like cells, and transdifferentiated cholangiocytes were observed in *Smad4* mutant mice (Figure S5A, S5B). To assess the enhancement of transdifferentiation, we further generated transition rates with the ratio of arrested LPCs, proliferating LPCs, hepatocyte-like cells or cholangiocytes to LPCs. Compared with control mice, *Smad4* mutant mice showed a declined LPC-hepatocyte-like transition rate and a similar LPC-cholangiocyte transition rate. On the other hand, LPC-arrestedLPC transition was suppressed and LPC-proliferatingLPC transition was elevated in *Smad4* mutant mice, indicating promoted proliferation of LPCs (Figure S5C). According to the results, we demonstrate that rather than advanced transdifferentiation, the accumulation of cholangiocytes in *Smad4* mutant mice is more likely resulted from increased LPC number due to the enhanced self-renewal.

***Onecut1* accumulates throughout LPC transition.**

As *Smad4* is considered not to affect hepatocyte-to-cholangiocyte transdifferentiation, only data from control mice were used in further analysis. In control mice, *Onecut1*$^+$ cells is observed only in a small proportion of hepatocytes, with expansion before and throughout LPC transition. Transdifferentiated hepatocyte-like cells showed almost complete loss of *Onecut1*$^+$ cells, while cholangiocytes showed mild loss of *Onecut1*$^+$ cells (Figure 3A). These results suggest a potential role of *Onecut1* during the LPC transition. In *Onecut1*$^+$ cells extracted from enriched clusters, *Onecut1* was gradually upregulated from hepatocytes to LPCs, and then was downregulated in cholangiocytes, with *Alb* downregulation and *Krt19* upregulation, showing a similar pattern with ONECUT1-EPs (Figure 3B). Compared to *Onecut1*$^-$ cells, *Onecut1*$^+$ cells showed decrease of hepatocytes, increase of preLPC.2s and LPCs, and consequently, LPC-number dependent increase of cholangiocytes, indicating that *Onecut1* facilitates LPC transition (Figure 3C, 3D). These results are consistent with that gradual overexpression of ONECUT1 in ONECUT1^{low}-EPs caused incomplete hepatocyte-to-cholangiocyte transdifferentiation. However, no remarkable differences of hepatic or cholangiocytic

markers were observed between *Onecut1*$^{-}$ and *Onecut1*$^{+}$ cells within same cell type (Figure 3E).

ONECUT1^{int}*Alb*^{low}*Krt19*^{low} dedifferentiated cells show high pulmonary metastatic potential.

As LPCs were considered as origin of metastasis-initiating cells, we performed *in vivo* metastasis assay to examine metastatic potential of ONECUT1-EPs. After 24 days of intravenous injection, pulmonary metastases were observed with ONECUT1^{int}-EPs and hepa1-6 cells, but not with ONECUT1^{low}-EPs or ONECUT1^{high}-EPs (Figure 4A, 4B). To confirm that high-level overexpression of ONECUT1 inhibits metastasis, we further introduced 3FLAG-ONECUT1 into metastatic hepa1-6 cells or ONECUT1-EP2s (Figure 4C). Both obtained cell lines showed downregulation of *Afp* mRNA, upregulation of *Krt19* mRNA, and decreased metastatic potential compared to parent cells, respectively (Figure 4D, 4E, 4F, 4G). These results indicate that metastatic potential acquisition is observed only in intermediate-ONECUT1-expressing cells with dedifferentiated traits.

LPCs present a “marker-less” phenotype.

None of the reported LPC or stem-cell markers distinguished preLPC.1s, preLPC.2s or LPCs in hepatocyte-to-cholangiocyte transdifferentiation continuum (Figure S6A). To identify the possible origin of metastasis-initiating cells, we tried to extract markers using single cell RNA-seq data. However, even with a loose cutoff (log2FC > 0.5 & p < 0.05), no preLPC.2 markers were extracted. *Mup20*, *Hsd17b13*, *Mug1*, *Hp*, *Itih3*, *Csad*, *Hpx* and *Apob* were extracted as preLPC.1 markers, indicating more hepatocyte-like traits. *Vim* and *Ltb* were extracted as LPC markers. Although *Csad* and *Vim* showed a lower background expression in hepatocyte-derived cells, expression in neighboring clusters were observed (Figure S6B, S6C).

As *Vim* is a key marker of epithelial-mesenchymal transition (EMT), we further assessed the expression of EMT marker genes. Epithelial score (epi_score) or mesenchymal score (mes_score) were respectively generated with epithelial or mesenchymal markers (Tan et al. 2014). Along with the transdifferentiation continuum, epi_score gradually increased, mes_score increased during LPC transition and retained in

transdifferentiated cells. Compared to LPCs, transdifferentiated hepatocyte-like cells showed similar epi_score, while cholangiocytes showed higher epi_score, suggesting that cholangiocyte maturation associates with possible mesenchymal-epithelial transition (MET). No decrease of epi_score or *Cdh1* loss was observed in hepatocyte-to-cholangiocyte transdifferentiation (Figure S6D). Among core transcription factors of EMT, only *Zeb2* was upregulated in a small proportion of LPCs (Figure S6E).

It is considerable that no specific markers were extracted, as the continuum indicates seamless transition states rather than different cell types. We further monitored continuous nature of gene expression during LPC transition with trajectory analysis. Along the pseudotime, preLPC.1s, preLPC.2s, LPCs and cholangiocytes overlapped with neighboring clusters (Figure S7A). *Cd24a*, *Sox4*, *Sox9*, and *Spp1* showed early increases, *Vim*, *Cd44* and *Epcam* increased later. At the end of continuum, *Sox9* and *Spp1* decreased, while *Krt19*, *Krt7* and *Tacstd2* (*Trop2*) rapidly elevated (Figure S7B).

Hepatically differentiated tumor cells acquire metastatic potential in early stage of LPC transition.

To investigate whether distant metastases show preLPC.2-like or LPC-like traits, we analyzed gene expression of distant metastases in human HCC. Microarray data were obtained from GSE40367 (Roessler et al. 2015). Normal liver samples were used as control due to complicated heterogeneity of primary tumor. A non-significant increase of *KRT19* were detected in distant metastases (Figure 5A). As distant metastases are clearly separated into two discrete groups with low or high *KRT19* expression, we further discussed the difference among normal livers, $KRT19^{low}$ and $KRT19^{high}$ distant metastases. Compared to normal liver, *ALB* and preLPC.1 marker *CSAD* decreased in both $KRT19^{low}$ and $KRT19^{high}$ metastases, while *KRT19* and LPC marker *VIM* increased exclusively in $KRT19^{high}$ metastases (Figure 5B). Six genes were further extracted with significant difference both between $KRT19^{low}$ / $KRT19^{high}$ metastases and between preLPC.2s / LPCs. All genes upregulated in $KRT19^{high}$ metastases (*Rgs5*, *Tmsb10*, *Tshz2*, *Slco3a1* and *Sparc*) also increased along the transdifferentiation pseudotime. Notably, *Rgs5* showed a peak expression in LPC state, while the only gene upregulated in $KRT19^{low}$ metastases, *Slc27a2*, decreased in preLPC.2 state, indicating preLPC.2-like

traits in *KRT19*^{low} metastases (Fig5C). The results revealed existence of both *ALB*^{low}*KRT19*^{low}*VIM*^{low} and *ALB*^{low}*KRT19*^{high}*VIM*^{high} distant metastases, suggesting metastatic potential acquisition in an earlier state during LPC transition, before upregulation of *KRT19* and *VIM*.

Discussion

Liver progenitor cells (LPCs) in adult liver are considered as hepatoblast-like progenitors with a bipotent capacity to differentiate into both hepatocytes and cholangiocytes. *Krt19*, *Epcam*, *Spp1* and *Sox9* are commonly used to characterize LPCs, but are difficult to distinguish them from cholangiocytes. In hepatocellular carcinoma, KRT19^{+} cells were reported to originate from hepatocytes, indicating existence of heptocyte-derived LPCs through transdifferentiation. The 3,5-diethoxycarbonyl-1,4-dihydrocollidine (DDC) diet model is widely used for study of hepatocyte-to-cholangiocyte transdifferentiation, in which hepatocyte-derived cells showed lack or low expression of mature cholagiocyte markers, indicating incomplete transdifferentiation (Tarlow et al. 2014). In 2021, Merrell *et al.* (Merrell et al. 2021) reported a DDC diet model with increased accumulation of KRT19^{+} cells by introducing mutant *Smad4*.

We tried to identify LPCs with the single cell RNA-seq data of eYFP-labeled hepatocyte-derived cells from DDC-treated control or *Smad4* mutant mice. The hepatocyte-derived cells formed a continuum from *Alb*^{high} cells to *Alb*^{low}*Krt19*$^{+}$ cells, indicating seamless states of hepatocyte-to-cholangiocyte transdifferneitation. Trajectory analysis revealed that a single cluster branches into *Alb*^{high} hepatocyte-like cells, *Krt19*$^{+}$ cholangiocytes and proliferating cells, suggesting LPC-like traits. We demonstrate that hepatocytes turn into LPCs through LPC transition, and then further differentiate into hepatocyte-like cells or cholangiocytes. Consistent with that SPP1^{+}MKI67^{+} hepatocyte-derived reactive ductules were reported as KRT19 negative (Schaub et al. 2018), proliferating cells were also diverged from LPCs but not cholangiocytes. Proliferating LPCs markedly increased in *Smad4* mutant mice, while ratio of cholangiocytes to LPCs showed to be similar between control and *Smad4* mutant mice, indicating the accumulation of cholangiocytes was resulted from enhanced self-renewal rather than differentiation of LPCs.

Agreed with reports from other groups, the common LPC markers failed to distinguish LPCs. In single cell RNA-seq data, only *Vim* was extracted as a LPC marker, which is also expressed in neighboring clusters and a wide range of cell types, indicating difficulties in identification of LPCs with markers *in vivo*. Although expression of *Vim* suggests transient mesenchymal traits during hepatocyte-to-cholangiocyte transdifferentiation, no typical EMT was observed.

By gradually expressing ONECUT1 in hepa1-6 derived ONECUT1^{low}*Alb*^{high}*Krt19*^{low} hepatocyte-like cells, we obtained ONECUT1^{int}*Alb*^{low}*Krt19*^{low} dedifferentiated cells and ONECUT1^{high}*Alb*^{low}*Krt19*^{high} cholangiocyte-like cells with downregulation of *Alb* and upregulation of *Krt19*. Although *Krt19* mRNA was upregulated in ONECUT1^{high}*Alb*^{low}*Krt19*^{high} cells, KRT19 protein expression was not detected, indicating impaired cholangiocyte maturation. On the other hand, knock down of ONECUT1 in hepa1-6 cells facilitated expression of KRT19 protein, which is in accord with premature cholangiocyte differentiation in ONECUT1 knockout mice (Clotman et al. 2002). During development, *Onecut1* is weakly expressed in liver parenchyma and accumulates in ductal plate (Clotman et al. 2002), and then is completely lost in mature cholangiocytes (Limaye et al. 2008). In single cell RNA-seq analysis, both accumulation of *Onecut1*$^{+}$ cells and *Onecut1* expression in *Onecut1*$^{+}$ cells increased before and throughout LPC transition, and then decreased in cholangiocytes. As similar behaviors were observed in all HCC cell model, development and DDC-treated mice, we demonstrate that *Onecut1* expression facilitates LPC transition, which could not be simply reversed by knock down of *Onecut1*. *Onecut1* in LPCs needs to be correctly regulated to determine cholangiocyte maturation, probably through TGFb signaling pathways (Clotman et al. 2005). Although ablation of *Smad4* resulted in accumulation of cholangiocytes, we consider that the effect is mainly dependent on disruption of growth inhibition by *Smad4*.

Despite accumulation of preLPC.2s and LPCs in *Onecut1*$^{+}$ cells, no remarkable differences of gene expression were observed between *Onecut1*$^{-}$ and *Onecut1*$^{+}$ cells within same cell type. *Onecut1*$^{-}$ cells could either be regulated by other pathways or be derived from expansion of *Onecut1*$^{+}$ cells with *Onecut1* loss (although *Onecut1* loss is suggested to associate with cholangiocyte maturation), which needs to be further

investigated. According to the result, we presume that cells within same cell type show similar traits regardless of whether *Onecut1* was expressed or not. Thus, we assume that ONECUT1-EPs model could partially represent LPC transition, but not only *Onecut1*$^{+}$ cells *in vivo*.

As LPCs are considered to be the origin of metastasis-initiating cells, we investigate metastatic potential of ONECUT1-EPs. As a result, only ONECUT1^{int}*Alb*^{low}*Krt19*^{low} dedifferentiated cells formed distant metastases. In microarray data of human HCC (Roessler et al. 2015), distant metastases showed both *ALB*^{low}*KRT19*^{low}*VIM*^{low} and *ALB*^{low}*KRT19*^{high}*VIM*^{high} traits. The results revealed that hepatically differentiated tumor cells acquire metastatic potential before *KRT19* and *VIM* upregulation, probably in preLPC.2 state. Although not suitable for identification, expression of cholangiocytic or mesenchymal markers in hepatocyte-derived cells could still be used to estimate the existence of preLPC.2 cells with metastatic potential. On the other hand, metastatic potential of LPCs has not been excluded due to the *ALB*^{low}*KRT19*^{high}*VIM*^{high} metastases, which could be resulted from either LPC-derived metastasis or further LPC transition of preLPC.2, or preLPC.2-derived metastases (Figure 5D).

LPC transition formed a seamless continuum, with most of the variable genes expressed intermediately between hepatocytes and cholangiocytes. Our study emphasizes the importance of *in vitro* study due to the marker-less phenotype in candidates of metastasis-initiating cells, preLPC.2s and LPCs. However, the multi-state ONECUT1-EP model could not represent the gradual transition correctly, and showed high expression variance among cell lines. We also generated inducible cell lines, but failed with *Alb* downregulation possibly due to the leakiness of ONECUT1. To further investigate metastatic characters during LPC transition and determination of terminal differentiation, sensitively-controlled inducible cell models need to be established.

In conclusion, consistent with ductal plate formation, we revealed LPC transition with *Onecut1* accumulation in both hepatocyte-to-cholangiocyte transdifferentiation and cell model, which possibly associates with transient acquisition of metastatic potential.

Methods

Cell lines. All cell lines were maintained in 10% FBS-containing DMEM at 37 °C in 5% CO_2. Cells were reseeded at 3 x 10^4 cells/cm^2 every 48 h. Stable clones were established by transfection of cells with pIRESEF1α/ONECUT1, pIRESEF1α/3FLAG-ONECUT1 or pSuper+/shONECUT1 plasmids using jetPEI (Polyplus, FR) and selection with neomycin (100-800 μg/ml), puromycin (0.5-4 μg/ml) or hygromycin (200-1600 μg/ml).

Immunoblotting and immunoprecipitation. For immunoblotting of cell lysates, cells were lysed in RIPA buffer. For immunoblotting of culture supernatants, regular culture medium was replaced with serum-free DMEM. Serum-free supernatants were collected 16 h later and concentrated with Amicon Ultra (MWCO, 3k, Merck Millipore, US). For immunoprecipitation, culture supernatants were collected after 48 h of incubation and filtered through 0.22-μm filters. Immunoprecipitation was performed with anti-ALB antibody (A90-134F-3, BETHYL, US) and protein G sepharose. Antibodies against ALB (ab207327, Abcam, UK), ONECUT1 (ab186743, Abcam, UK), KRT19 (ab52625, Abcam, UK) and ACTIN (MAB1501, Merck Millipore, US) were used in immunoblotting. CBB Stain One (Nacalai tesque, JP) was used for total protein staining.

RNA isolation and quantitative reverse transcription (RT) PCR. Total RNA was extracted with Sepasol-RNA I Super G (Nacalai tesque, JP), followed by reverse transcription using ReverTra Ace qPCR RT Master Mix (TOYOBO, JP) and purification by ethanol precipitation. mRNA expression was determined by real-time PCR using THUNDERBIRD SYBR qPCR Mix (TOYOBO, JP) and StepOnePlus (Applied Biosystems, US), and then normalized to GAPDH expression. Primer sequences for quantitative RT-PCR are shown in Supplementary Table.

Immunofluorescence analyses. For immunofluorescence analysis, cells were cultured in 24-well dishes for 48 or 72 h and fixed with 10% formalin, followed by permeabilization with 0.5% Triton X-100. After blocking in 5% BSA, cells were incubated with anti-KRT19 antibody (ab52625, Abcam, UK) overnight at 4 °C, followed by incubation with TRITC-labeled anti-rabbit IgG for 1 h at room temperature, and then

incubated with FITC-labeled anti-ALB antibody (A90-134F-3, BETHYL, US) overnight at 4 °C. All images were acquired using the BZ-9000 BIOREVO fluorescence microscope (Keyence, JP).

Mice, xenograft and *in vivo* metastasis assay. Balb/c nude mice (male, 6-week-old, SLC, JP) were used for *in vivo* studies. For xenograft assay, 2 x 10^6 cells were injected into flanks of nude mice. Tumor volume was calculated as Length x $(\text{Width})^2$ / 2. For *in vivo* metastasis assay, 2 x 10^6 cells were injected into tail vein of nude mice. Lungs were collected after 24 days, followed by fixation with 10% formalin. For each mouse, 2 or 3 sections separated by 0.5 mm were used for haematoxylin and eosin staining. Metastatic burden was calculated as (counts of metastatic foci) / (tissue area). All animal experiments were reviewed and approved by the Animal Committee of Kyoto University.

Single cell RNA-seq analysis. Filtered gene data were obtained from GSE157698. Low quality cells and genes were filtered with min.cells = 3, 200 < nFeatures < 4000, and percent.MT < 40. Bulk liver parenchyma from control mice (GSM4885630 and GSM4885634), *eYFP*$^+$ bulk liver parenchyma from *Smad4* mutant mice (GSM4885631 and GSM4885635, *eYFP* > 0.2), and YFP$^+$ sorted cells from both control mice (GSM4885632 and GSM4885636) and *Smad4* mutant mice (GSM4885633 and GSM4885637) were integrated with Seurat (Hao et al. 2021). RunUMAP visualization were used for clustering at resolution = 0.7. Monocle3 or Monocle2 (Qiu et al. 2017) were used for trajectory analysis of whole continuum or LPC transition, respectively.

Microarray analysis. CEL files were obtained from GSE40367 (Roessler et al. 2015) and processed by Affymetrix Expression Console Software using the MicroArray Suite 5 (MAS5) method. Outliers were removed with Tukey's method.

Statistics. Statistical analyses were performed using Graphpad Prism, Microsoft Excel or R. Data were represented by mean ± s.d., *P*-values of statistical significance were represented as * $P < 0.05$; ** $P < 0.01$; *** $P < 0.001$; **** $P < 0.0001$ unless otherwise indicated.

Acknowledgments

We thank the Center for Anatomical, Pathological and Forensic Medical Research, Kyoto University Graduate School of Medicine, for preparing microscope slides.

Figure legends

Figure 1. Gradual expression of ONECUT1 in ONECUT1^{low} cells facilitates incomplete hepatocyte-to-cholangiocyte transdifferentiation. (A) Morphology of mouse HCC cell line hepa1-6, epithelial-like hepaEP1 and hepaEP2 cell lines derived from hepa1-6. **(B)** Expression of hepatic markers determined by quantitative RT-PCR. mRNA level of hepa1-6 was set to 1, n = 3, * indicates significant difference, 1-way ANOVA. **(C)** Immunoblotting of secreted ALB (upper) and total protein staining (lower). **(D)** Expression of liver-enriched transcription factors determined by quantitative RT-PCR. mRNA level of hepa1-6 was set to 1, n = 3, * indicates significant difference, 1-way ANOVA. **(E, F)** Immunoblotting of ONECUT1 (upper) and ACTIN (lower). **(G)** Quantification of protein levels in (F). Protein level of hepa1-6 was set to 1, n = 5, different letters indicate significant differences, 1-way ANOVA. **(H, I)** Expression of hepatic or cholangiocytic markers determined by quantitative RT-PCR. mRNA level of hepaEP1 was set to 1, n = 3, * indicates significant difference, 1-way ANOVA.

Figure 2. Hepatocyte-to-cholangiocyte transdifferentiation continuum. (A) Single cell RNA-seq profiling of hepatocyte-derived cells, by cluster. **(B)** Trajectory analysis of hepatocyte-derived cells. **(C)** Expression of *Alb*, *Krt19*, *Cdkn1a* and *Mki67* in hepatocyte-derived cells. **(D)** Hepatocyte-to-cholangiocyte transdifferentiation continuum, by cell type. **(E)** Relative scores of hepatic or cholangiocytic markers, by cluster.

Figure 3. Enrichment and expression of *Onecut1* during LPC transition. (A) Accumulation of *Onecut1*$^{+}$ cells with hep_score and chol_score in control mice, by cluster. **(B)** Expression of *Onecut1* in *Onecut1*$^{+}$ cells extracted from enriched clusters, by cell type. **(C)** Proportions of *Onecut1*$^{-}$ or *Onecut1*$^{+}$ cells, by cell type. **(D)** Ratio of proportions between *Onecut1*$^{-}$ and *Onecut1*$^{+}$ cells, by cell type. **(E)** Expression of indicated genes in *Onecut1*$^{-}$ or *Onecut1*$^{+}$ cells, by cell type.

Figure 4. ONECUT1^{int}*Alb*^{low}*Krt19*^{low} cells show high pulmonary metastatic potential. (A) Haematoxylin and eosin staining of lungs, 24 days after intravenous injection. **(B)** Relative metastatic burden in lungs. Metastatic burden of hepa1-6 was set to 1, n = 3 for hepa1-6, ONECUT1-EP2, ONECUT1-EP7 or ONECUT1-EP9, n = 4 for hepaEP1 or ONECUT1-EP1, n = 5 for hepaEP2, different letters indicate significant differences, 1-way ANOVA. **(C)** Immunoblotting of ONECUT1 (upper) and ACTIN (lower). **(D)** Expression of *Alb*, *Afp* and *Krt19* determined by quantitative RT-PCR. mRNA level of hepa1-6 was set to 1, n = 3, * indicates significant difference, t-test. **(E)** Expression of *Alb*, *Afp* and *Krt19* determined by quantitative RT-PCR. mRNA level of ONECUT1-EP2 was set to 1, n = 3, * indicates significant difference, t-test. **(F)** Haematoxylin and eosin staining of lungs and relative metastatic burden. Metastatic burden of hepa1-6 was set to 1, n = 3, * indicates significant difference, t-test. **(G)** Haematoxylin and eosin staining of lungs and relative metastatic burden. Metastatic burden of ONECUT1-EP2 was set to 1, n = 3, * indicates significant difference, t-test.

Figure 5. preLPC.2-like and LPC-like distant metastases in human HCC (A) Expression of *KRT19* in normal liver or distant metastases. Non-significant, t-test. **(B)** Expression of *ALB*, *CSAD*, *KRT19* and *VIM* in normal liver, *KRT19*^{low} metastases or *KRT19*^{high} metastases. Outliers were removed using Tukey's method, * indicates significant difference, 1-way ANOVA. **(C)** Expression of common differentially expressed genes, with expression curve along pseudotime (left), or expression in human HCC data (right). * indicates significant difference, t-test. **(D)** Schema of LPC transition in hepatocyte-to-cholangiocyte transdifferentiation, with possible metastatic potential acquisition.

Figure S1. (A) Immunoprecipitation of secreted ALB in serum-containing culture supernatants. **(B)** *In vitro* proliferation assay. Cell count of time 0 was set to 1, n = 19, * indicates significant difference, 2-way RM ANOVA. **(C)** Tumor xenograft assay in nude mice. n = 4, non-significant, 2-way RM ANOVA. **(D)** Immunoblotting of secreted ALB (upper) and total protein staining (lower).

Figure S2. (A) Immunoblotting of ONECUT1 (upper) and ACTIN (lower). **(B)** Expression of hepatic or cholangiocytic markers determined by quantitative RT-PCR.

mRNA level of hepa1-6 was set to 1, n = 3, * indicates significant difference, t-test. **(C, D)** Immunofluorescence staining of ALB (green) and KRT19 (red). **(E)** Immunoblotting of KRT19 (upper) and ACTIN (lower).

Figure S3. (A) Single cell RNA-seq profiling of hepatocyte-derived cells, by cluster. **(B)** Expression of *Krt19* in hepatocyte-derived cells, by cluster, arrows indicate estimated cholangiocyte clusters. **(C)** Expression of hepatic markers, cholangiocytic markers, hepatic stellate cell markers, endothelial cell markers and Kupffer cell markers.

Figure S4. Expression of hepatic or cholangiocytic markers used in calculating scores, and cellcycle markers.

Figure S5. (A) Hepatocyte-to-cholangiocyte transdifferentiation continuum of control or *Smad4* mutant mice, by cell type. **(B)** Proportions of control or *Smad4* mutant mice, by cell type. **(C)** Transition rates of control or *Smad4* mutant mice, by cell type.

Figure S6. (A) Expression of reported LPC markers, by cell type. **(B)** Venn diagram of upregulated genes in preLPC.1s, preLPC.2s or LPCs. **(C)** Expression of common upregulated genes extracted in (B), by cell type. **(D)** Relative scores of epithelial or mesenchymal markers and expression of *Cdh1* and *Cdh2*, by cluster. **(E)** Expression of core EMT transcription factors and *Vim*, by cell type.

Figure S7. (A) Distribution of cells in LPC transition, by cell type. **(B)** Expression curve along pseudotime of hepatic markers, cholangiocytic markers, and LPC markers.

References

Cameron, M. D., E. E. Schmidt, N. Kerkvliet, K. V. Nadkarni, V. L. Morris, A. C. Groom, A. F. Chambers, and I. C. MacDonald. 2000. “Temporal progression of metastasis in lung: cell survival, dormancy, and location dependence of metastatic inefficiency.” *Cancer Res* 60 (9): 2541–6.

Chakrabarti, R., J. Hwang, M. Andres Blanco, Y. Wei, M. Lukačišin, R. A. Romano, K. Smalley, et al. 2012. “Elf5 inhibits the epithelial-mesenchymal transition in mammary gland development and breast cancer metastasis by transcriptionally repressing Snail2.” *Nat Cell Biol* 14 (11): 1212–22.

Chaudhary, K., O. B. Poirion, L. Lu, and L. X. Garmire. 2018. “Deep Learning-Based Multi-Omics Integration Robustly Predicts Survival in Liver Cancer.” *Clin Cancer Res* 24 (6): 1248–59.

Cheung, W. K., M. Zhao, Z. Liu, L. E. Stevens, P. D. Cao, J. E. Fang, T. F. Westbrook, and D. X. Nguyen. 2013. “Control of alveolar differentiation by the lineage transcription factors GATA6 and HOPX inhibits lung adenocarcinoma metastasis.” *Cancer Cell* 23 (6): 725–38.

Clotman, F., P. Jacquemin, N. Plumb-Rudewiez, C. E. Pierreux, P. Van der Smissen, H. C. Dietz, P. J. Courtoy, G. G. Rousseau, and F. P. Lemaigre. 2005. “Control of liver cell fate decision by a gradient of TGF beta signaling modulated by Onecut transcription factors.” *Genes Dev* 19 (16): 1849–54.

Clotman, F., V. J. Lannoy, M. Reber, S. Cereghini, D. Cassiman, P. Jacquemin, T. Roskams, G. G. Rousseau, and F. P. Lemaigre. 2002. “The onecut transcription factor HNF6 is required for normal development of the biliary tract.” *Development* 129 (8): 1819–28.

Franzén, O., L. M. Gan, and J. L. M. Björkegren. 2019. “PanglaoDB: a web server for exploration of mouse and human single-cell RNA sequencing data.” *Database (Oxford)* 2019 (January).

Govaere, O., M. Komuta, J. Berkers, B. Spee, C. Janssen, F. de Luca, A. Katoonizadeh, et al. 2014. “Keratin 19: a key role player in the invasion of human hepatocellular carcinomas.” *Gut* 63 (4): 674–85.

Guo, X., L. Xiong, T. Sun, R. Peng, L. Zou, H. Zhu, J. Zhang, H. Li, and J. Zhao. 2012. “Expression features of SOX9 associate with tumor progression and poor prognosis of hepatocellular carcinoma.” *Diagn Pathol* 7 (April): 44.

Hao, Y., S. Hao, E. Andersen-Nissen, W. M. Mauck, S. Zheng, A. Butler, M. J. Lee, et al. 2021. “Integrated analysis of multimodal single-cell data.” *Cell* 184 (13): 3573–87.

Kouros-Mehr, H., S. K. Bechis, E. M. Slorach, L. E. Littlepage, M. Egeblad, A. J. Ewald, S. Y. Pai, I. C. Ho, and Z. Werb. 2008. “GATA-3 links tumor differentiation and dissemination in a luminal breast cancer model.” *Cancer Cell* 13 (2): 141–52.

Lazarevich, N. L., O. A. Cheremnova, E. V. Varga, D. A. Ovchinnikov, E. I. Kudrjavtseva, O. V. Morozova, D. I. Fleishman, N. V. Engelhardt, and S. A. Duncan. 2004. “Progression of HCC in mice is associated with a downregulation in the expression of hepatocyte nuclear factors.” *Hepatology* 39 (4): 1038–47.

Li, C. M., V. Gocheva, M. J. Oudin, A. Bhutkar, S. Y. Wang, S. R. Date, S. R. Ng, et al. 2015. “Foxa2 and Cdx2 cooperate with Nkx2-1 to inhibit lung adenocarcinoma metastasis.” *Genes Dev* 29 (17): 1850–62.

Limaye, P. B., G. Alarcón, A. L. Walls, M. A. Nalesnik, G. K. Michalopoulos, A. J. Demetris, and E. R. Ochoa. 2008. “Expression of specific hepatocyte and cholangiocyte transcription factors in human liver disease and embryonic development.” *Lab Invest* 88 (8): 865–72.

Luzzi, K. J., I. C. MacDonald, E. E. Schmidt, N. Kerkvliet, V. L. Morris, A. F. Chambers, and A. C. Groom. 1998. “Multistep nature of metastatic inefficiency: dormancy of solitary cells after successful extravasation and limited survival of early micrometastases.” *Am J Pathol* 153 (3): 865–73.

Merrell, A. J., T. Peng, J. Li, K. Sun, B. Li, T. Katsuda, M. Grompe, K. Tan, and B. Z. Stanger. 2021. “Dynamic Transcriptional and Epigenetic Changes Drive Cellular Plasticity in the Liver.” *Hepatology* 74 (1): 444–57.

Mu, X., R. Español-Suñer, I. Mederacke, S. Affò, R. Manco, C. Sempoux, F. P. Lemaigre, et al. 2015. “Hepatocellular carcinoma originates from hepatocytes and not from the progenitor/biliary compartment.” *J Clin Invest* 125 (10): 3891–3903.

Pan, H. W., Y. H. Ou, S. Y. Peng, S. H. Liu, P. L. Lai, P. H. Lee, J. C. Sheu, C. L. Chen, and H. C. Hsu. 2003. “Overexpression of osteopontin is associated with intrahepatic metastasis, early recurrence, and poorer prognosis of surgically resected hepatocellular carcinoma.” *Cancer* 98 (1): 119–27.

Qiu, X., Q. Mao, Y. Tang, L. Wang, R. Chawla, H. A. Pliner, and C. Trapnell. 2017. “Reversed graph embedding resolves complex single-cell trajectories.” *Nat Methods* 14 (10): 979–82.

Roessler, S., G. Lin, M. Forgues, A. Budhu, S. Hoover, R. M. Simpson, X. Wu, et al. 2015. “Integrative genomic and transcriptomic characterization of matched primary and metastatic liver and colorectal carcinoma.” *Int J Biol Sci* 11 (1): 88–98.

Schaub, J. R., K. A. Huppert, S. N. T. Kurial, B. Y. Hsu, A. E. Cast, B. Donnelly, R. A. Karns, et al. 2018. “De novo formation of the biliary system by TGFβ-mediated hepatocyte transdifferentiation.” *Nature* 557 (7704): 247–51.

Sun, H., H. Tang, D. Xie, Z. Jia, Z. Ma, D. Wei, L. Mishra, et al. 2016. “Krüppel-like Factor 4 Blocks Hepatocellular Carcinoma Dedifferentiation and Progression through Activation of Hepatocyte Nuclear Factor-6.” *Clin Cancer Res* 22 (2): 502–12.

Sun, Y. F., Y. Xu, X. R. Yang, W. Guo, X. Zhang, S. J. Qiu, R. Y. Shi, B. Hu, J. Zhou, and J. Fan. 2013. “Circulating stem cell-like epithelial cell adhesion molecule-positive tumor cells indicate poor prognosis of hepatocellular carcinoma after curative resection.” *Hepatology* 57 (4): 1458–68.

Tan, T. Z., Q. H. Miow, Y. Miki, T. Noda, S. Mori, R. Y. Huang, and J. P. Thiery. 2014. “Epithelial-mesenchymal transition spectrum quantification and its efficacy in deciphering survival and drug responses of cancer patients.” *EMBO Mol Med* 6 (10): 1279–93.

Tarlow, B. D., C. Pelz, W. E. Naugler, L. Wakefield, E. M. Wilson, M. J. Finegold, and M. Grompe. 2014. “Bipotential adult liver progenitors are derived from chronically injured mature hepatocytes.” *Cell Stem Cell* 15 (5): 605–18.

Walter, T. J., C. Vanderpool, A. E. Cast, and S. S. Huppert. 2014. “Intrahepatic bile duct regeneration in mice does not require Hnf6 or Notch signaling through Rbpj.” *Am J Pathol* 184 (5): 1479–88.

Winslow, M. M., T. L. Dayton, R. G. Verhaak, C. Kim-Kiselak, E. L. Snyder, D. M. Feldser, D. D. Hubbard, et al. 2011. “Suppression of lung adenocarcinoma progression by Nkx2-1.” *Nature* 473 (7345): 101–4.

Figure 1

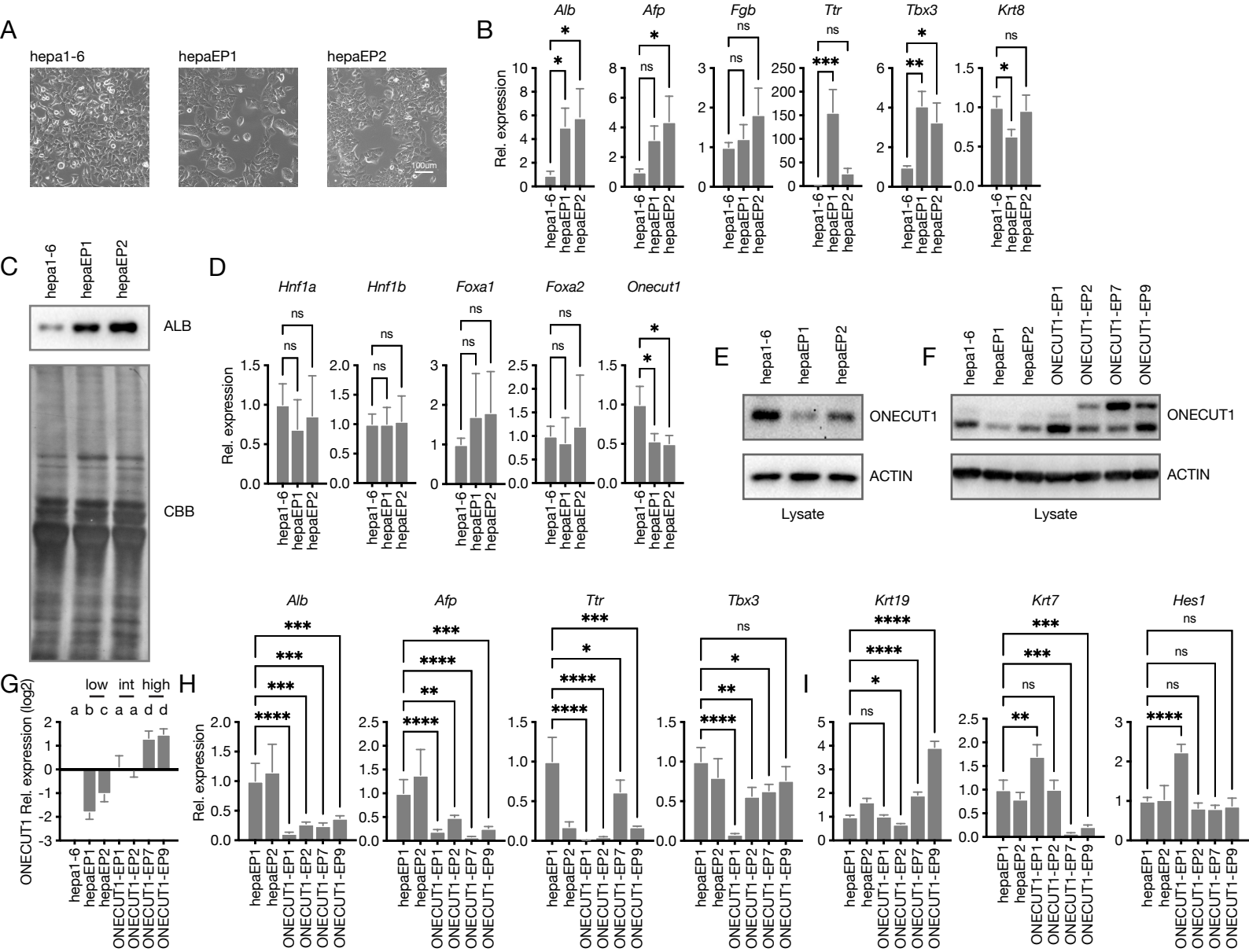
A
hepa1-6
hepaEP1
hepaEP2
100µm
B
Alb
Afp
Fgb
Ttr
Tbx3
Krt8
Rel. expression
hepa1-6
hepaEP1
hepaEP2
C
hepa1-6
hepaEP1
hepaEP2
ALB
CBB
D
Hnf1a
Hnf1b
Foxa1
Foxa2
Onecut1
Rel. expression
E
hepa1-6
hepaEP1
hepaEP2
ONECUT1
ACTIN
Lysate
F
hepa1-6
hepaEP1
hepaEP2
ONECUT1-EP1
ONECUT1-EP2
ONECUT1-EP7
ONECUT1-EP9
ONECUT1
ACTIN
Lysate
G
low
int
high
a b c a a d d
ONECUT1 Rel. expression (log2)
hepa1-6
hepaEP1
hepaEP2
ONECUT1-EP1
ONECUT1-EP2
ONECUT1-EP7
ONECUT1-EP9
H
Alb
Afp
Ttr
Tbx3
Rel. expression
I
Krt19
Krt7
Hes1
hepaEP1
hepaEP2
ONECUT1-EP1
ONECUT1-EP2
ONECUT1-EP7
ONECUT1-EP9

Figure 2

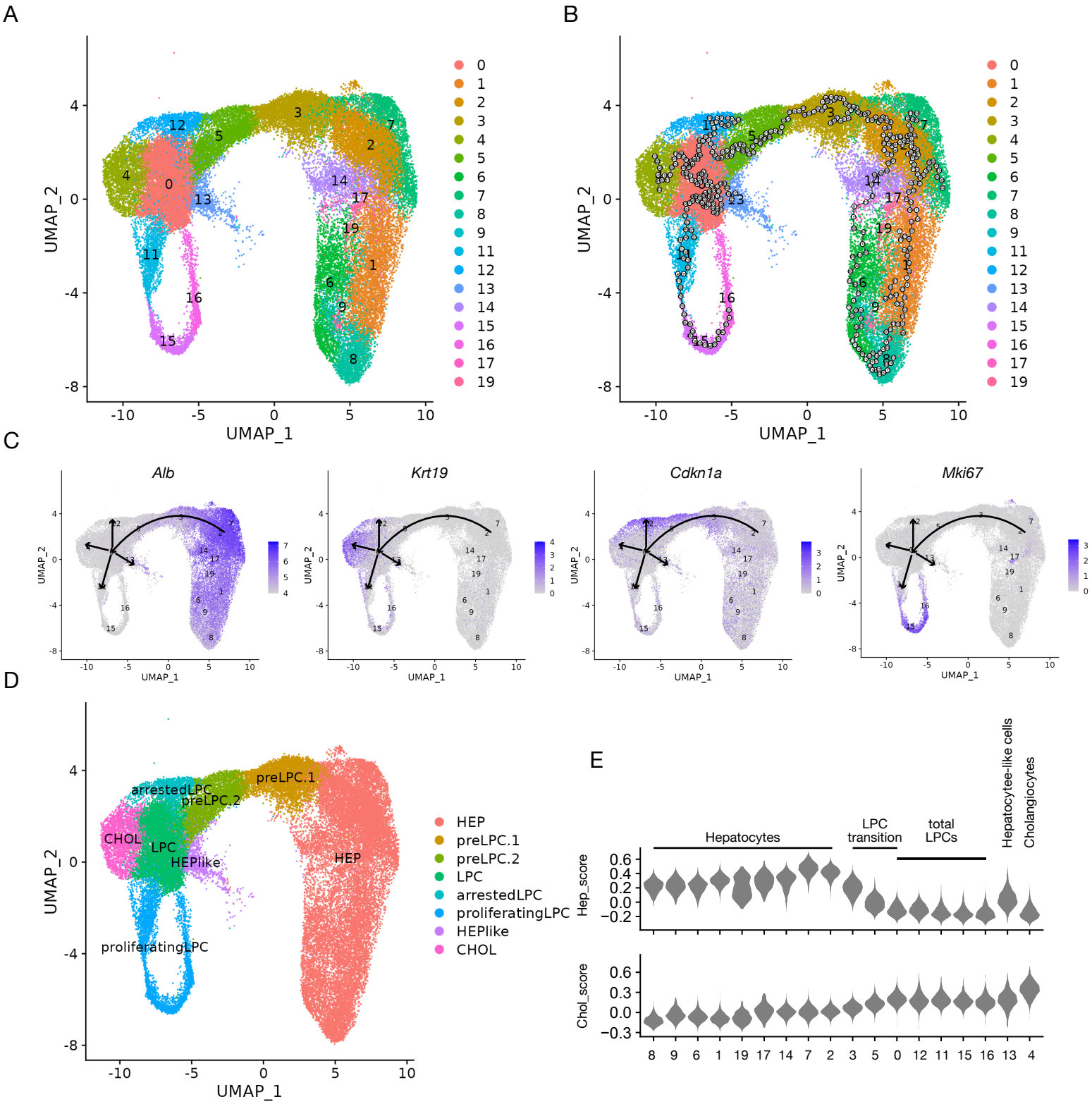
A
B
C
D
E
UMAP_1
UMAP_2
0
1
2
3
4
5
6
7
8
9
11
12
13
14
15
16
17
19
Alb
Krt19
Cdkn1a
Mki67
HEP
preLPC.1
preLPC.2
LPC
arrestedLPC
proliferatingLPC
HEPlike
CHOL
Hepatocytes
LPC transition
total LPCs
Hepatocytee-like cells
Cholangiocytes
Hep_score
Chol_score

Figure 3

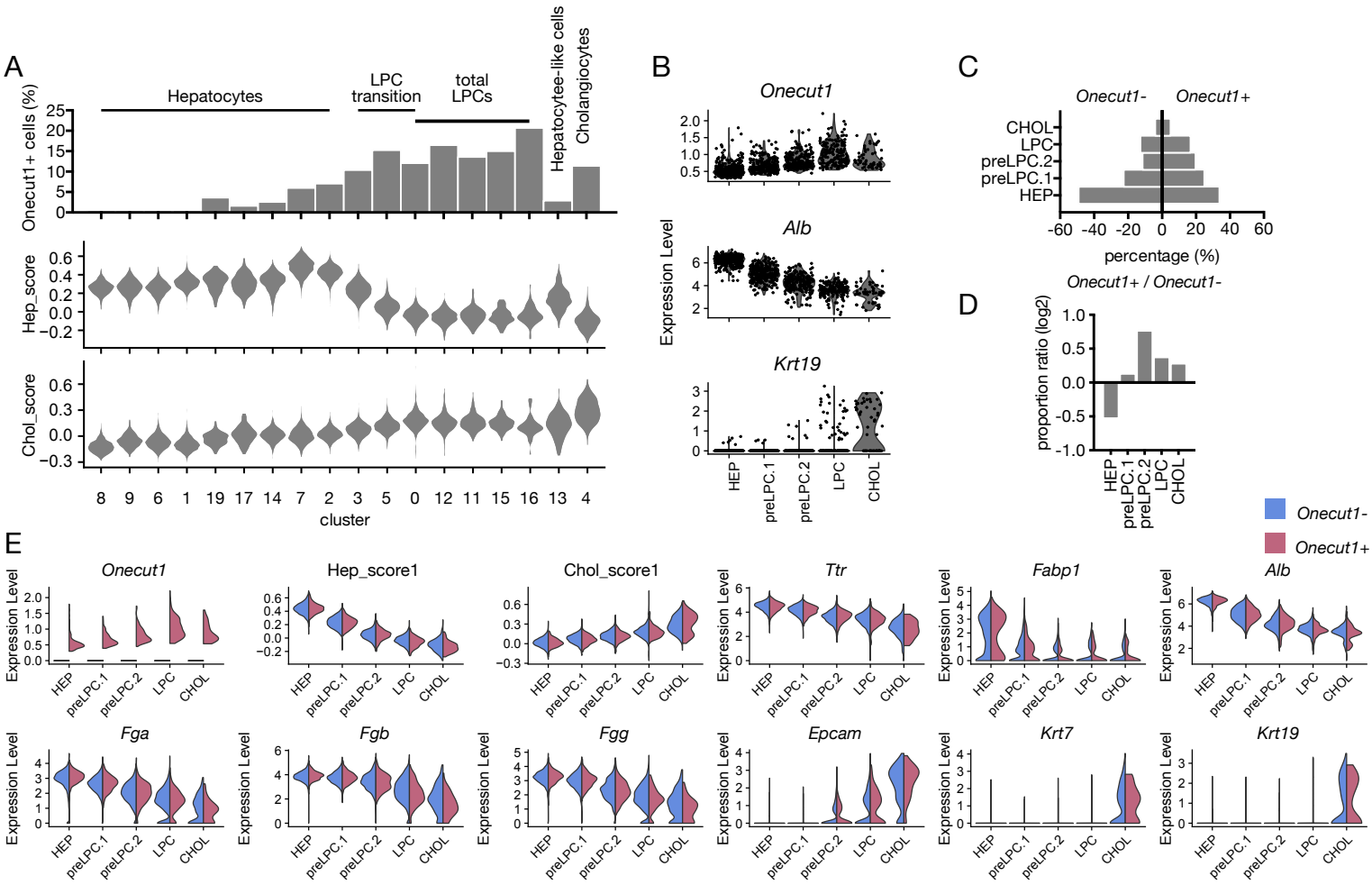
A
Hepatocytes
LPC transition
total LPCs
Hepatocytee-like cells
Cholangiocytes
Onecut1+ cells (%)
Hep_score
Chol_score
8 9 6 1 19 17 14 7 2 3 5 0 12 11 15 16 13 4
cluster
B
Onecut1
Alb
Krt19
Expression Level
HEP
preLPC.1
preLPC.2
LPC
CHOL
C
Onecut1-
Onecut1+
CHOL
LPC
preLPC.2
preLPC.1
HEP
percentage (%)
D
Onecut1+ / Onecut1-
proportion ratio (log2)
Onecut1-
Onecut1+
E
Onecut1
Hep_score1
Chol_score1
Ttr
Fabp1
Alb
Fga
Fgb
Fgg
Epcam
Krt7
Krt19

Figure 4

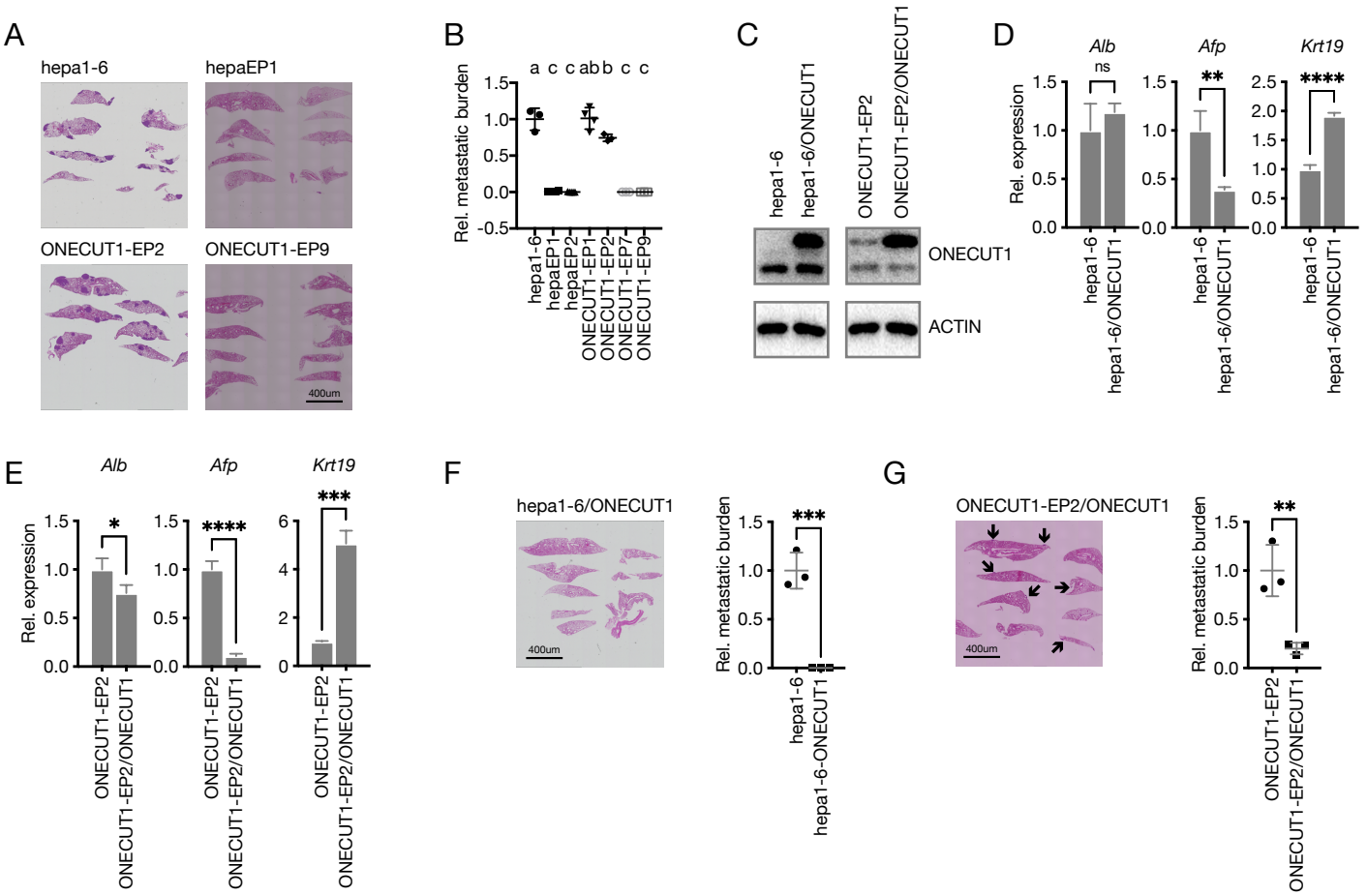
A
hepa1-6
hepaEP1
ONECUT1-EP2
ONECUT1-EP9
400um
B
Rel. metastatic burden
a c c ab b c c
hepa1-6
hepaEP1
hepaEP2
ONECUT1-EP1
ONECUT1-EP2
ONECUT1-EP7
ONECUT1-EP9
C
hepa1-6
hepa1-6/ONECUT1
ONECUT1-EP2
ONECUT1-EP2/ONECUT1
ONECUT1
ACTIN
D
Alb
Afp
Krt19
Rel. expression
ns
**
****
hepa1-6
hepa1-6/ONECUT1
E
Alb
Afp
Krt19
Rel. expression
*
****
***
ONECUT1-EP2
ONECUT1-EP2/ONECUT1
F
hepa1-6/ONECUT1
400um
Rel. metastatic burden
***
hepa1-6
hepa1-6-ONECUT1
G
ONECUT1-EP2/ONECUT1
400um
Rel. metastatic burden
**
ONECUT1-EP2
ONECUT1-EP2/ONECUT1

Figure 5

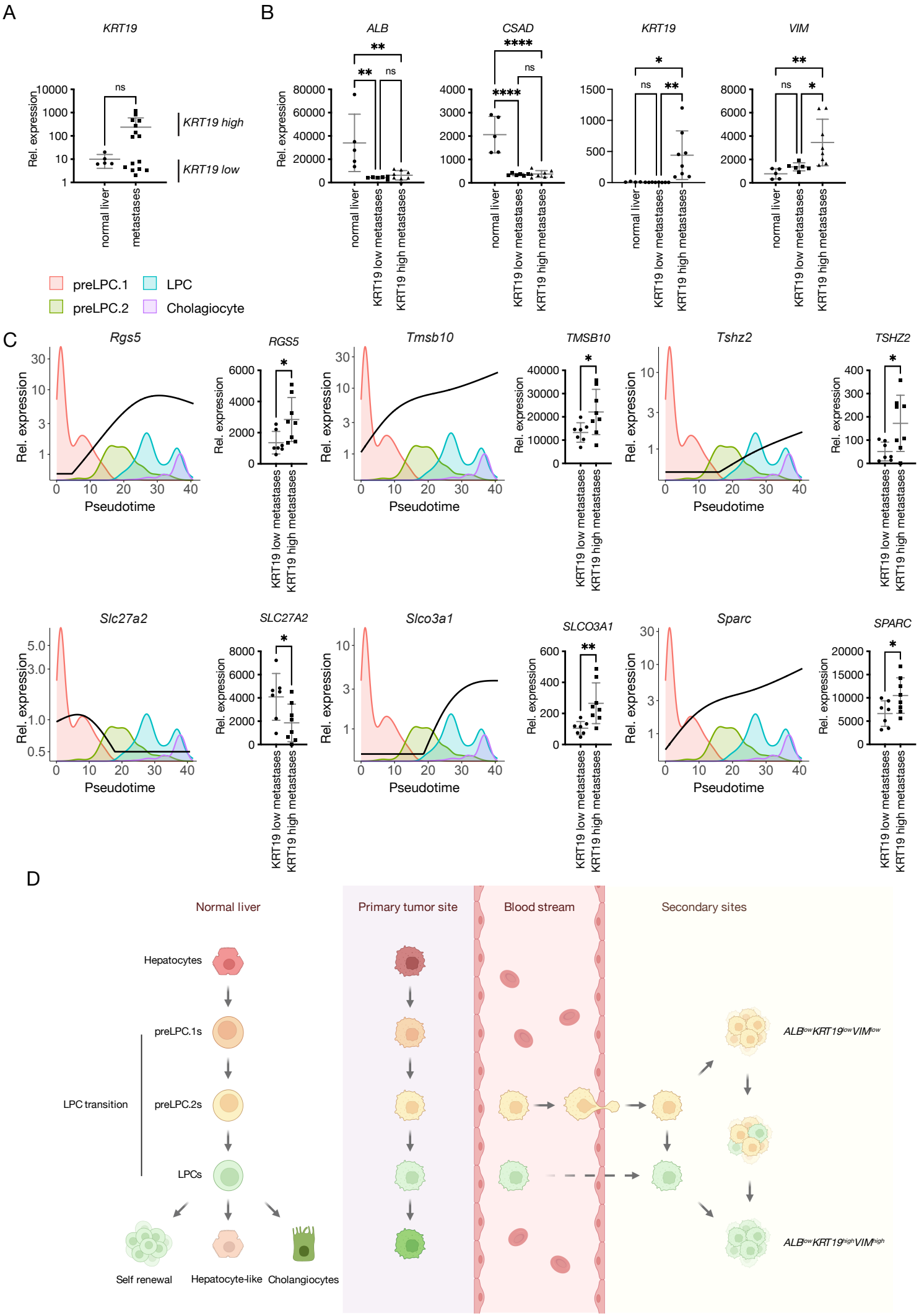
A
KRT19
Rel. expression
ns
KRT19 high
KRT19 low
normal liver
metastases
preLPC.1
preLPC.2
LPC
Cholagiocyte
B
ALB
CSAD
KRT19
VIM
normal liver
KRT19 low metastases
KRT19 high metastases
C
Rgs5
RGS5
Tmsb10
TMSB10
Tshz2
TSHZ2
Slc27a2
SLC27A2
Slco3a1
SLCO3A1
Sparc
SPARC
Pseudotime
D
Normal liver
Primary tumor site
Blood stream
Secondary sites
Hepatocytes
preLPC.1s
preLPC.2s
LPCs
LPC transition
Self renewal
Hepatocyte-like
Cholangiocytes
ALBlowKRT19lowVIMlow
ALBlowKRT19highVIMhigh